Forest Ecology and Management 524 (2022) 120515

Contents lists available at ScienceDirect

Forest Ecology and Management

journal homepage: www.elsevier.com/locate/foreco

Assessing spatial patterns and drivers of burn severity in subtropical forests in Southern China based on Landsat 8

Lingling Guo [a,b,c], Shun Li [a,b,c,*], Zhiwei Wu [a,b,c,*], Russell A. Parsons [f], Shitao Lin [d], Bo Wu [c], Long Sun [e]

[a] Key Laboratory of Poyang Lake Wetland and Watershed Research, Ministry of Education, Jiangxi Normal University, Nanchang 330022, PR China
[b] Key Laboratory of Natural Disaster Monitoring, Early Warning and Assessment of Jiangxi province, Jiangxi Normal University, Nanchang 330022, PR China
[c] School of Geography and Environment, Jiangxi Normal University, Nanchang 330022, PR China
[d] Forestry Department, Jiangxi Environmental Engineering Vocational College, Ganzhou 341000, PR China
[e] School of Forestry, Northeast Forestry University, Harbin 150040, PR China
[f] USDA Forest Service, Rocky Mountain Research Station, Missoula Fire Sciences Laboratory, 5775 Highway 10 West Missoula, MT 59808, USA

ARTICLE INFO

Keywords:
Burn severity
Spatial patterns
Spectral indices
Landsat 8 OLI
Subtropical forests
Composite burn index

ABSTRACT

Burn severity assessment is vital for the development of effective fire management strategies. Subtropical forests in Southern China support rich forest resources but are also disturbed by frequent forest fires, resulting in varying burn severity areas. However, the lack of accuracy assessment of burn severity based on spectral indices has limited our understanding of spatial patterns and drivers of burn severity in this region and the implementation of effective forest fire management. In this study, we compared the accuracy of different spectral indices from Landsat 8 Operational Land Imager (OLI) in assessing burn severity. Moreover, the optimal spectral index was selected to map burn severity and analyze its spatial patterns and drivers by using the random forest model. The results showed that (1) dNBR, RdNBR, and RBR outperformed the others in accuracy of fitting burn severity, and dNBR was slightly higher in accuracy classification; (2) vegetation (pre-fire NDVI) and human activity (distance to the nearest road or settlement) were the most important drivers affecting burn severity patterns; (3) the proportion of moderate and low burn severity was higher, and most burn areas were concentrated near settlements and roads, but areas with higher burn severity tended to be distributed in uphill, sunny slopes, and high altitudes. In view of this, we recommend targeted forest fire management according to the distribution pattern and drivers of burn severity in this region, including setting up fire belts near residential areas and roads, and prioritizing fuel removal plans in areas prone to develop higher burn severity.

1. Introduction

Wildfire is one of the main disturbances in a forest, which has an important influence on the patterns and processes of forest landscapes (Lorente et al., 2013; Bowd et al., 2019; Brewer et al., 2005). Detailed and accurate information on the spatial patterns of burn severity is critical to understand changes in ecological processes and landscape patterns caused by forest fires, as well as our ability to manage forest fires (Steel et al., 2018; McLauchlan et al., 2020). Subtropical forests are prone to fire in China (Jin et al., 2017; Yu et al., 2014a), and unlike other forest types, they usually have smaller average burned areas but high fire frequency (Su et al., 2019). However, the spatial patterns and drivers of burn severity of subtropical forests in China are still insufficiently understood, and the relatively small size and scattered distribution of burned areas may be a challenge for the burn severity assessment of subtropical forests.

Burn severity is mainly assessed based on tree mortality, canopy and trunk destruction, char height, and soil and ash color changes (Key and Benson, 2005), but field assessment is labor-intensive and impractical to cover and map the extensive spatial patterns of burn severity. Remote sensing technology is widely used in burn severity evaluation; it can assess burn severity by analyzing the change in spectral reflectance before and after fires (Ramsey and Arrowsmith, 2001). In particular, the visible, near-infrared, and short-wave infrared spectral bands are sensitive to fire disturbance, which is an important basis for identifying burned areas and evaluating burn severity (Soverel et al., 2010).

* Corresponding authors at: School of Geography and Environment, Jiangxi Normal University, 99 Ziyang Road, Nanchang 330020, China.
E-mail addresses: lishun@jxnu.edu.cn (S. Li), wuzhiwei@jxnu.edu.cn (Z. Wu).

https://doi.org/10.1016/j.foreco.2022.120515
Received 7 May 2022; Received in revised form 3 August 2022; Accepted 30 August 2022
Available online 13 September 2022
0378-1127/

Previous studies have developed several spectral indices and composite burn index (CBI) regression models to quantitatively evaluate burn severity (Fernández-Manso and Quintano, 2015; García-Llamas et al., 2020; Hayes and Robeson, 2011). These indices usually have high predictive accuracy in the assessment of burn severity with large burn sizes and clear boundaries (Fernández-García et al., 2022). However, the relatively small average burned area and high fire frequency in subtropical forests lead to irregular and scattered burned areas (Su et al., 2019). These characteristics not only cause great uncertainty in the estimation of burn severity based on the spectral indices but also make it difficult to assess the spatial patterns of burn severity in subtropical forest regions. A spectral index in assessing burn severity varies greatly across burned areas and ecosystem types (boreal and subtropical forests) (Kurbanov et al., 2017). Therefore, it is necessary to further explore the effectiveness of different spectral indices in burn severity assessment to better understand the spatial patterns of burn severity in subtropical forests.

Three types of spectral indices are usually used to assess burn severity: (1) reflective indices (Cardil et al., 2019; Miller and Thode, 2007b; Parks et al., 2014), such as normalized burn ratio (NBR), differenced NBR (dNBR), relative differenced NBR (RdNBR), relativized burn ratio (RBR), normalized difference vegetation index (NDVI), difference NDVI (dNDVI), enhanced vegetation index (EVI), and difference EVI (dEVI); (2) thermal metrics (Yu et al., 2014b; Zheng et al., 2016), including land surface temperature (LST) and difference LST (dLST); and (3) mixed indices (Zheng et al., 2016), such as LST/EVI and d(LST/EVI). Currently, the most widely used indices are NBR-based improved indices, such as RdNBR and RBR, which have advantages in assessing burn severity (Cardil et al., 2019; Whitman et al., 2018). However, whether these indices are suitable for evaluating burn severity in subtropical forests and whether the evaluation results meet the accuracy requirements need to be further verified.

The spatial pattern of burn severity is often driven by vegetation, topography, and climate or weather (Fang et al., 2015; Fernández-García et al., 2022; Lentile et al., 2006). Climate or weather is usually considered to play a key role in burn severity distribution on a broad scale, whereas terrain and vegetation are the main drivers affecting the heterogeneity of spatial patterns of burn severity at the local scale (Wu et al., 2013; Liu et al., 2012). Topography influences fire behavior by altering microclimatic conditions and forest characteristics (Broncano and Retana, 2004), leading to different spatial patterns of burn severity. Certain aspects of vegetation characteristics, such as type, structure, and load, have important effects on fire occurrence and behavior (Birch et al., 2015). Various local environmental factors influence the spatial patterns of burn severity across the landscape, but the degree to which they influence require to be further detected (Cansler and McKenzie, 2012; Harvey et al., 2016). Generally, the influence of environmental drivers on burn severity varies greatly in different regions. However, the spatial patterns of burn severity in subtropical forests are still poorly understood. To provide a scientific basis for forest fire prevention management, more information on the spatial patterns and drivers of burn severity in subtropical forests is necessary.

The goals of this study were to assess and compare the ability of different spectral indices in assessing burn severity, and to map and clarify the spatial patterns and drivers of burn severity in subtropical forests. The main steps included (1) establishing regression models between the spectral indices from Landsat 8 Operational Land Imager (OLI) and the field survey data (CBI assessment results), and selecting the optimal spectral indices for burn severity assessment by comparison; (2) analyzing the spatial patterns and drivers of burn severity in the study area using the random forest model based on the selected optimal spectral index.

2. Materials and methods

2.1. Study area

The study area was located in the southern part of Jiangxi Province, China (Fig. 1). It covered an area of approximately 39,000 km^2, with an elevation of 0–1960 m. The area has a typical subtropical monsoon climate, with a mean annual temperature of 19.3 °C and a mean annual precipitation of 1600 mm. Forest coverage reached 76 %, and the dominant tree species include Masson pine (*Pinus massoniana*) and Chinese fir (*Cunninghamia lanceolata*). Among these fuel types, Masson pine trees are oily and more flammable than other trees. Because of the high population density and well-developed road network, forest fires in the study area are mainly caused by human fire. The forest fire protection period is usually from October to April, and most forest fires occurred from January to April.

2.2. Research framework

We used CBI (Table A1) to investigate 10 forest fire events (Table A2) in the study area, from which 420 field samples of burn severity were obtained. Landsat 8 OLI (L1T processing level) remote sensing imagery within 1 year after the fire event was downloaded from the United States Geological Survey (USGS) website (https://glovis.usgs.gov/app) (Table A3). Landsat 8 OLI image preprocessing, including radiation calibration and atmospheric correction, was performed using ENVI. We used the ‘raster’ package (Hijmans, 2022) of R software (R Core Team, 2017) to calculate 12 spectral indices, including NBR, dNBR, RdNBR, RBR, NDVI, dNDVI, EVI, dEVI, LST, dLST, LST/EVI, and d(LST/EVI). In this study, 70 % of the field survey data was used as training samples to establish regression models (linear, quadratic polynomial, cubic polynomial, logarithmic, and saturated growth). The coefficient of determination (R^2) and root mean square error (RMSE) were used to evaluate the accuracy of the five models in determining the relationship between CBI and spectral indices, and the remaining 30 % of the field survey data was used to generate a confusion matrix (overall accuracy and kappa coefficient) to evaluate the prediction accuracy of burn severity. According to the accuracy assessment, the optimal index was selected to map the spatial patterns of burn severity. The random forest model was used to analyze the relative importance of their drivers (terrain, NDVI, and human activity). Partial dependence plots were used to further illustrate the effects of variables on spatial patterns of burn severity. A flowchart outlining the proposed methodology is shown in Fig. 2.

2.3. Data collection and processing

2.3.1. Field surveys

Ten fire events that occurred from 2020 to 2021 in the southern part of Jiangxi were considered. All fire events mainly occurred in Masson pine and fir forests at an altitude of 90–644 m and a slope of 0–49° (Table A4).

CBI was used for field sampling (Key and Benson, 2005) (Table A1). Field surveys of burned areas were conducted within 1 year after the occurrence of a fire event. To ensure that the pixels of the measured CBI and Landsat 8 OLI images were consistent in spatial location and size, 30 m × 30 m plots were used in field surveys. These plots were distributed in areas with different terrain conditions and burn severities. Each plot was divided into four layers according to vertical height: A, representing the surface combustible material and soil layer; B, representing herbs, short shrubs, and small trees (<1 m height); C, representing tall shrubs and trees (>1–5 m height); and D, representing forest canopy (>5 m) (Key and Benson, 2005). Each layer had 4–5 variables that were visually estimated in the range 0 to 3: 0 (unburned), 1 (low burn severity), 2 (moderate burn severity), and 3 (high burn severity). The estimated value of each layer synthesis was performed to obtain CBI of the entire plot.

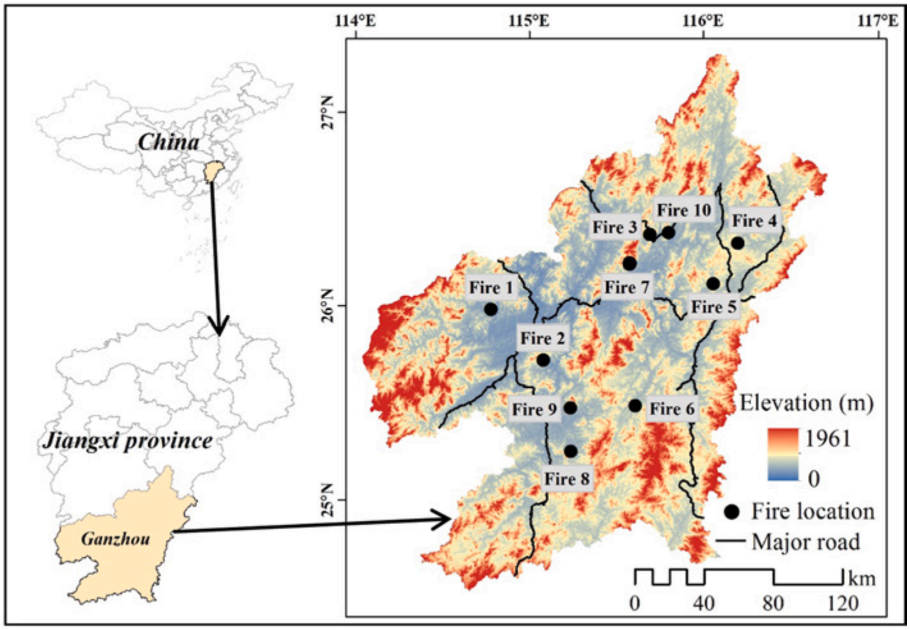

Fig. 1. Study area and major recent fire sites.

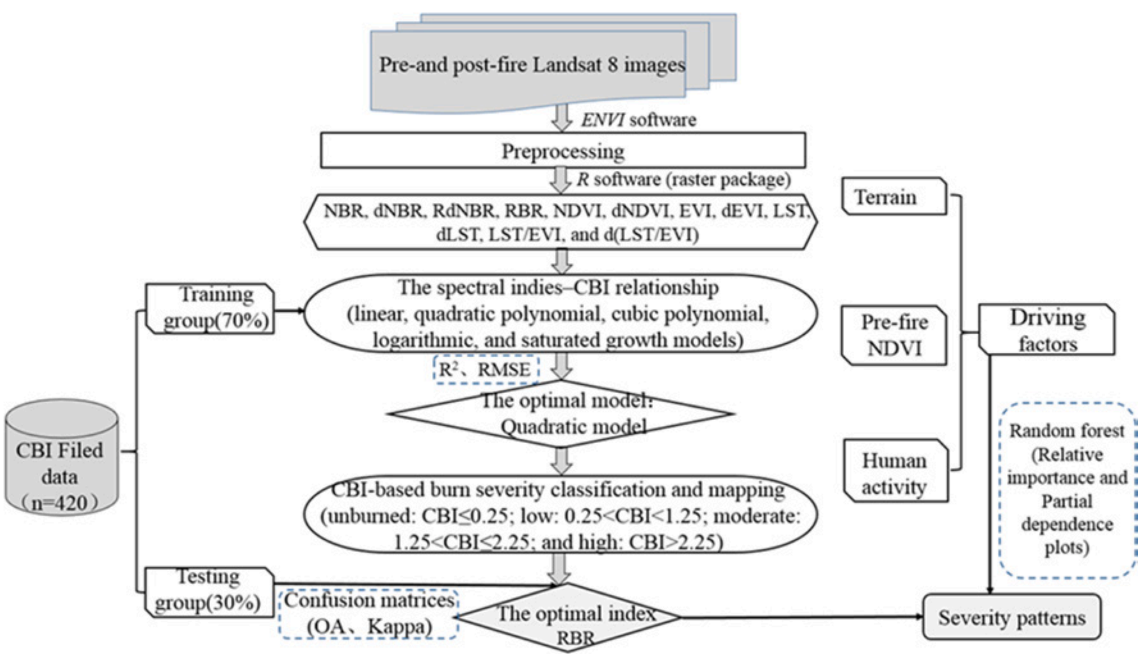

Fig. 2. Flowchart of the methodology used in the study.

CBI of each layer was calculated using the following formula:

$$\mathrm{CBI_i} = \sum_{j=1}^{n} \mathrm{X_{ij}}/n \tag{1}$$

where CBI_i is the composite burn index for stratum i; X_{ij} is the severity grade score for factor j in stratum I; and n is the total number of factors in stratum i.

CBI of each sample plot was calculated using the following formula:

$$\mathrm{CBI} = \sum_{i=1}^{K} \mathrm{CBI_i}/\mathrm{k} \tag{2}$$

where CBI is the composite burn index for a plot surveyed; CBI_i is the composite burn index for stratum I; and k is the total number of burned strata in the plot surveyed.

We obtained 420 CBI data samples from January to September 2021 and randomly divided them into two groups, with 70 % of the samples used to construct the regression model and 30 % used to verify the accuracy of the model (Table 1). The sample distributions of different CBI thresholds met the requirements of model construction and accuracy verification.

2.3.2. Remote sensing data

Landsat 8 OLI (L1T processing level) provided by the USGS is a digital number geometrically rectified and radiometrically corrected; thus, only radiometric calibration and atmospheric correction were needed for multispectral data analysis. The FLAASH module provided in the ENVI 5.3 environment was used to calibrate the panchromatic band.

Table 1
Statistics of the composite burn index (CBI) of all field plots.

Burn severity	Class boundary, CBI	Number (train/test)	Minimum	Maximum	Mean	SD
Unburned	[0, 0.25]	102 (72/30)	0	0.24	0.01	0.04
Low	[0.25, 1.25]	123 (85/38)	0.3	1.25	0.87	0.27
Moderate	[1.25, 2.25]	119 (88/31)	1.26	2.25	1.86	0.33
High	[2.25, 3]	76 (49/27)	2.28	3	2.57	0.23

To better identify burned patches, the spatial resolution of Landsat 8 OLI multispectral data was set at 15 m by using automatic registration and image fusion of multispectral and panchromatic data. To keep the spatial resolution of each band consistent, other bands (SWIR and thermal) were also resampled to achieve a spatial resolution of 15 m.

R software was used to individually analyze the preprocessed images. Reflective indices, including NBR, dNBR, RdNBR, RBR, NDVI, dNDVI, EVI, and dEVI; thermal metrics, including LST and dLST; and mixed indices, including LST/EVI and d(LST/EVI), were then determined (Table 2).

2.3.3. Spatial drivers of burn severity

Topography data. A 30-m spatial resolution grid was derived using digital elevation model (DEM) data obtained from the China Geospatial Data Cloud Platform (https://www.gscloud.cn/). In the ArcGIS 10.3 environment, the spatial analysis function was used to extract altitude, slope, aspect, and slope position.

Vegetation data. Pre-fire NDVI was selected as vegetation factors to analyze the potential drivers of burn severity (Fu et al., 2020). It was derived from Landsat 8 data with a spatial resolution of 30 m.

Human activity-related data. Distance from the nearest road and distance from the nearest settlement are important variables of fire occurrence and spread (Liu et al., 2012). Road data of China was obtained from the website of the National Basic Geographic Information Center (1:250,000, https://www.ngcc.cn/ngcc/). Settlement points data of Ganzhou city in 2020 was obtained from the Data Center of Resources and Environmental Sciences of Chinese Academy of Sciences (https://www.resdc.cn/). In the ArcGIS 10.3 environment, the spatial analysis function was used to calculate the Euclidean distance from each pixel to the nearest road or settlement with a spatial resolution of 30 m, which was considered the distance to the nearest road or settlement.

2.4. Data analysis

2.4.1. Model construction and accuracy evaluation

Linear, quadratic polynomial, cubic polynomial, logarithmic, and saturated growth models (eq. (1)–(5)) were used to analyze the relationships between CBI (independent variable) and spectral indices (dependent variable).

$$\text{Linear model}: y = a(x) + b \tag{3}$$

$$\text{Quadratic polynomial model}: y = a(x)^2 + b(x) + c \tag{4}$$

$$\text{Cubic polynomial model}: y = a(x)^3 + b(x)^2 + c(x) + d \tag{5}$$

$$\text{Logarithmic model}: y = aln(x) + b \tag{6}$$

$$\text{Saturated growth model}: y = x(a|x| + b)^{-1} \tag{7}$$

where $\times$ is the CBI value, and y is the burn severity index.

R^2 and RMSE were used to evaluate the fitting ability of the model using the training and validation sets. Different CBI thresholds presented sample distributions that meet the requirements of model construction and accuracy verification.

Burn severity was divided into four grades: unburned (CBI $\leq$ 0.25), low severity (0.25 $<$ CBI $\leq$ 1.25), moderate severity (1.25 $<$ CBI $\leq$ 2.25),

Table 2
Spectral indices used to evaluate burn severity.

Spectral index	Landsat 8 OLI OLI/TIRS formula	Reference
NBR	(b5 − b7)/(b5 + b7)	(López-García and Caselles, 1991)
dNBR	NBRpre − NBRpost	(Key and Benson, 2005)
RdNBR	dNBR/(|NBRpre|$^{0.5}$)	(Miller and Thode, 2007)
RBR	dNBR/(NBRpre + 1.001)	(Parks et al., 2014)
NDVI	(b5 − b4)/(b5 + b4)	(Rouse et al., 1973)
dNDVI	NDVIpre-NDVIpost	(Zhu et al., 2006)
EVI	2.5(b5 − b4)/(b5 + 6b4 + 7.5b2 + 1)	(Gao et al., 2000)
dEVI	EVIpre-EVIpost	(Zhu et al., 2006)
LST	LST in Kelvin from b10(ts)	(Yu *et al.*, 2014)
dLST	LSTpost − LSTpre	(Zheng *et al.*, 2015)
LST/EVI	(LST − 273.15)/EVI	(Zheng *et al.*, 2015)
d(LST/EVI)	$(LST/EVI)_{post}/(LST/EVI)_{pre}$	(Zheng *et al.*, 2015)

Note: b4, b5, and b7 are the surface reflectance values measured in the visible (red), near-infrared, and shortwave infrared bands of the Landsat 8 OLI sensor, respectively.

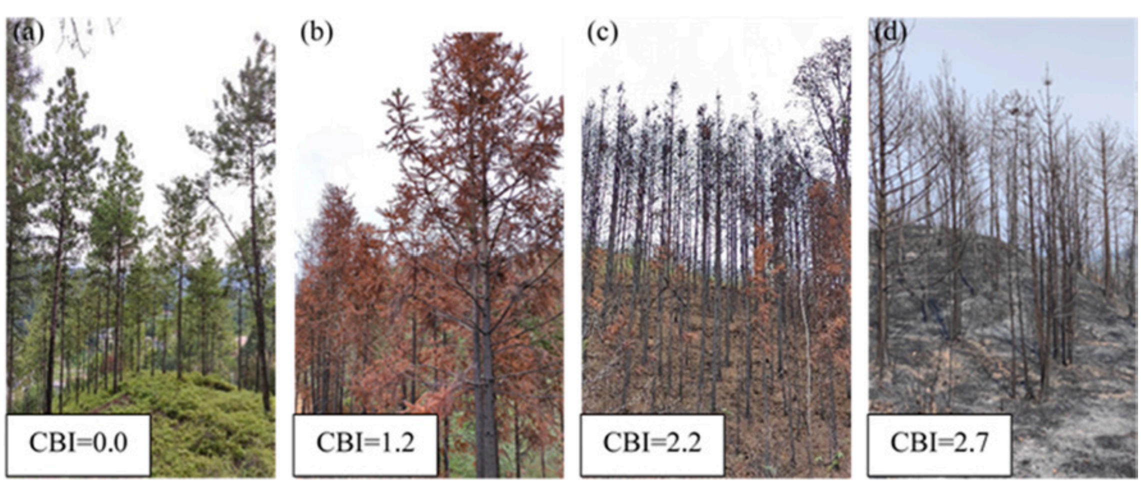

Fig. 3. Examples of the four classes of burn severity in a subtropical forest in Southern China. (a) Unburned; (b) low severity; (c) moderate severity; and (d) high severity.

and high severity (CBI > 2.25) (Kurbanov et al., 2017; Miller and Thode, 2007a).

A confusion matrix was used to evaluate the accuracy of the automatic identification of burn severity. The evaluation indicators were overall accuracy and kappa. Overall accuracy is the ratio of the total number of pixels correctly classified by the classifier to the total number of pixels. Kappa integrates production accuracy and user accuracy. Larger overall accuracy and kappa values indicate the difference between classification results. When the actual measurement is smaller, the classification accuracy of the classifier is higher.

Overall accuracy was calculated using the following formula:

$$OA = \frac{\mathrm{TP} + \mathrm{TN}}{TP + \mathrm{FN} + FP + \mathrm{TN}} \quad (8)$$

where TP is a positive sample correctly classified by the model (predicted as 1 and is actually 1); FN is a positive sample incorrectly classified by the model (predicted as 0 but is actually 1); FP is a negative sample incorrectly classified by the model (predicted as 1 but is actually 0); and TN is a negative sample correctly classified by the model (predicted as 0 and is actually 0).

The kappa coefficient was calculated using the following formula:

$$Kappa = \frac{\mathrm{N}\sum_{i=1}^{r}\mathrm{X}_{ii} - \sum_{i=1}^{r}(\mathrm{x}_{i+} \times \mathrm{x}_{+i})}{N^2 - \sum_{i=1}^{r}(\mathrm{x}_{i+} \times \mathrm{x}_{+i})} \quad (9)$$

where N is the total number of pixels of all real references; X_{ii} is the diagonal value of the confusion matrix; and X_{i+} and X_{+i} are the sums of each row and column of the confusion matrix.

2.4.2. Analysis of spatial patterns and drivers

Based on the optimal index and model selected by the above methods, the distribution map of burn severity in this study area was obtained. All spatial pattern and driver analyses are based on the acquired burn severity distribution maps (Fig. 5). In the analysis of spatial patterns and drivers, the relative impact and marginal effect of each driver on the spatial pattern of burn severity were evaluated using random forest regression analysis (Liaw and Wiener, 2002). To determine the relative importance of each driver (terrain, vegetation, human activity) to burn severity, we utilized the percentage increase in the mean square error (%IncMSE) in random forest regression analysis (De Keersmaecker et al., 2015). Larger %IncMSE values imply higher factor importance to burn severity. Furthermore, the partial dependence plots in random forest regression analysis were used to visualize the relationship between the drivers and burn severity (Schwalm et al., 2017). All these data analyses were performed using the randomForest package in R (Liaw and Wiener, 2002).

3. Results

3.1. Accuracy assessment of burn severity

The comparison results indicated that RdNBR and RBR ($R^2 = 0.74$, RMSE < 0.2) outperformed other indices in burn severity assessment (Fig. 4 and Table 3). Second only to these two indices, dNBR also has high fitting accuracy ($R^2 = 0.68$, RMSE < 0.15). Among the several regression models, the linear model, quadratic polynomial model, and cubic polynomial model showed good fitting effect (Fig. 4 and Table 3), indicating that these three models have better performance in fitting the regression relationship between spectral index and burn severity. Table 4..

Among the three optimal spectral indices selected above, the overall accuracy of burn severity was close to 0.6, and the kappa coefficient was up to 0.44 (Table 5). dNBR was slightly better in overall classification accuracy (0.58) and kappa coefficient (0.44) than the other two indices. These indices had higher user's accuracy for unburned areas (0.77), whereas moderate burn severity was lower (0.48). Although the fitting results of RBR and RdNBR were better, dNBR performed slightly better in user's accuracy. All three indices can be used as potential optimal indices for burn severity assessment in this area.

3.2. Burn severity mapping and spatial pattern analysis

According to the dNBR-derived burn severity mapping, burned areas were grouped into four severity classes (unburned to high burn severity) (Fig. 5). In our study area, burn severity was mainly low and moderate, accounting for>70 % of the total burned area, and the proportion of high burn severity was relatively small (167.38 ha, accounting for 21.16 %) (Table 6).

Due to the drivers of terrain, vegetation, and human activities, burn

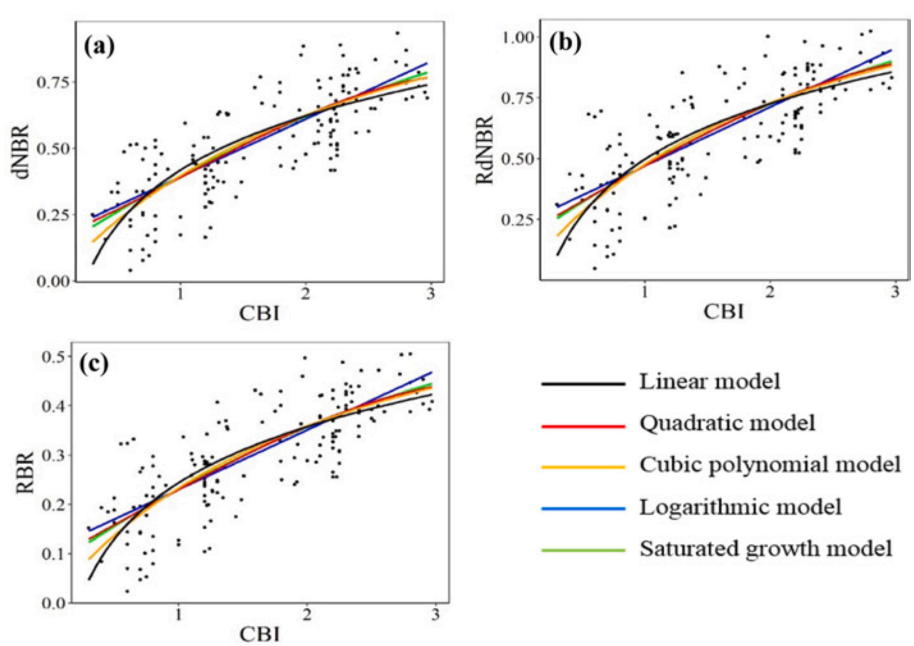

Fig. 4. Scatterplots representing the modeled relationships of CBI with dNBR, RdNBR, and RBR using the five models. (a) Differenced normalized burn ratio (dNBR). (b) Relative differenced normalized burn ratio (RdNBR). (c) Relativized burn ratio (RBR).

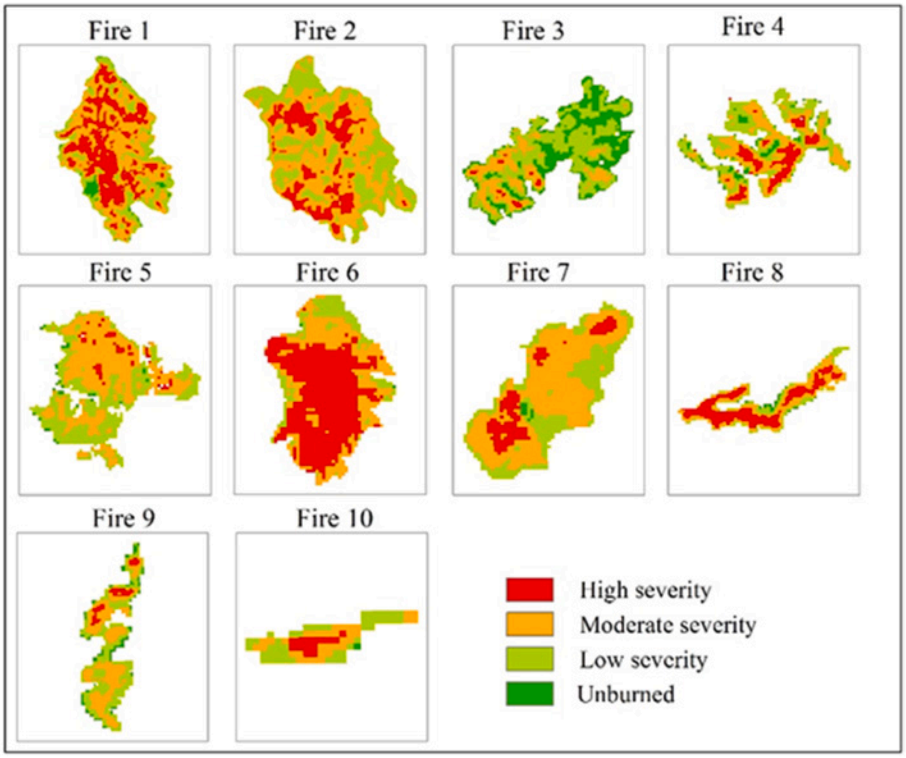

Fig. 5. Burn severity maps obtained using dNBR derived from Landsat 8 OLI imagery.

Table 3
Results of independent validation using the observed CBI and different burn severity indices.

Model	Linear		Quadratic polynomial		Cubic polynomial		Logarithmic		Saturated growth	
Spectral indices	R^2	RMSE	R^2	RMSE	R^2	RMSE	R^2	RMSE	R^2	RMSE
NBR	0.535	0.166	0.546	0.165	0.546	0.165	0.332	0.159	0.897	0.336
dNBR	**0.674**	0.145	**0.676**	0.145	**0.677**	0.145	0.575	0.126	0.593	0.124
RdNBR	**0.726**	0.159	**0.737**	0.156	**0.737**	0.157	0.567	0.143	**0.693**	0.169
RBR	**0.729**	0.078	**0.739**	0.077	**0.739**	0.077	0.574	0.070	**0.695**	0.083
NDVI	0.283	0.178	0.283	0.178	0.283	0.179	0.204	0.168	2.123	0.371
dNDVI	0.133	2.411	0.183	2.344	0.195	2.331	0.338	0.142	0.341	0.141
EVI	0.002	3.376	0.032	3.331	0.060	3.289	0.053	3.683	0.341	0.141
dEVI	0.056	3.683	0.057	3.688	0.063	3.685	0.081	3.376	0.043	3.445
LST	0.106	0.722	0.156	0.703	0.259	0.660	0.038	0.733	0.054	0.727
dLST	0.031	1.677	0.062	1.653	0.116	1.608	0.043	1.768	0.059	1.753
LST/EVI	0.009	1.458	0.011	1.460	0.015	1.459	0.027	1.622	NA	NA
d(LST/EVI)	0.003	1.434	0.014	1.429	0.014	1.432	0.018	1.581	0.017	1.581

Table 4
dNBR, RdNBR, and RBR model-derived thresholds and corresponding field-measured CBI thresholds.

Severity grade	CBI	dNBR	RdNBR	RBR
Unburned	0–0.25	<0.214	<0.22	<0.108
Low	0.25–1.25	0.214–0.455	0.22–0.544	0.108–0.267
Moderate	1.25–2.25	0.455–0.665	0.544–0.778	0.267–0.383
High	2.25–3	>0.665	>0.778	>0.383

Table 5
Confusion matrix of Landsat 8 OLI burn severity classification using different burn severity indices (dNBR, RdNBR, and RBR).

Spectral index	Unburned	Low	Moderate	High	Overall accuracy	Kappa
dNBR	0.77	0.50	0.48	0.60	0.58	0.44
RdNBR	0.70	0.53	0.45	0.60	0.56	0.42
RBR	0.70	0.53	0.42	0.60	0.56	0.41

severity varied significantly in spatial patterns across the landscape (Fig. 6). The relative importance of various factors in random forest regression analysis showed that vegetation (pre-fire NDVI) (%IncMSE = 237.44) was the most important factor affecting the pattern distribution of burn severity. Human activity (distance to the nearest road; %IncMSE = 218.78) was also of great importance to burn severity, followed by elevation (%IncMSE = 188.12), slope (%IncMSE = 176.76), distance to the nearest settlement (%IncMSE = 168.85), aspect (%IncMSE = 151.94), and slope position (%IncMSE = 73.04) (Fig. 6).

The partial dependence plots (Fig. 7) and percentage plots (Fig. 8) characterized the impact of different drivers on the spatial pattern distribution of burn severity. Burn severity was closely related to pre-fire NDVI, and burn severity was obviously higher when NDVI was in the range 0.8–1.0 (Fig. 7). The distance to the nearest road also positively

Table 6
Distribution of burned areas in the four burn severity classes based on the dNBR index.

Fire event ID	Burn severity class Unburned (ha)	(%)	Low (ha)	(%)	Moderate (ha)	(%)	High (ha)	(%)	Total (ha)
1	7.45	2.75	65.88	24.32	117.32	43.30	80.28	29.63	270.92
2	0.20	0.08	96.71	39.32	107.19	43.58	41.87	17.02	245.97
3	24.32	32.69	36.00	48.38	12.94	17.39	1.15	1.54	74.41
4	2.70	7.40	16.45	45.07	11.88	32.55	5.47	14.98	36.50
5	0.68	1.99	15.21	44.83	16.67	49.14	1.37	4.05	33.93
6	0.05	0.14	4.39	13.42	10.33	31.59	17.93	54.85	32.69
7	0.27	0.85	10.06	31.55	17.64	55.33	3.92	12.28	31.88
8	0.90	2.83	6.41	20.16	11.27	35.43	13.23	41.58	31.82
9	2.70	8.80	14.27	46.52	11.86	38.66	1.85	6.02	30.67
10	0.02	1.08	0.99	47.31	0.77	36.56	0.32	15.05	2.09
Total	39.29	**4.97**	266.36	**33.68**	317.86	**40.19**	167.38	**21.16**	790.88

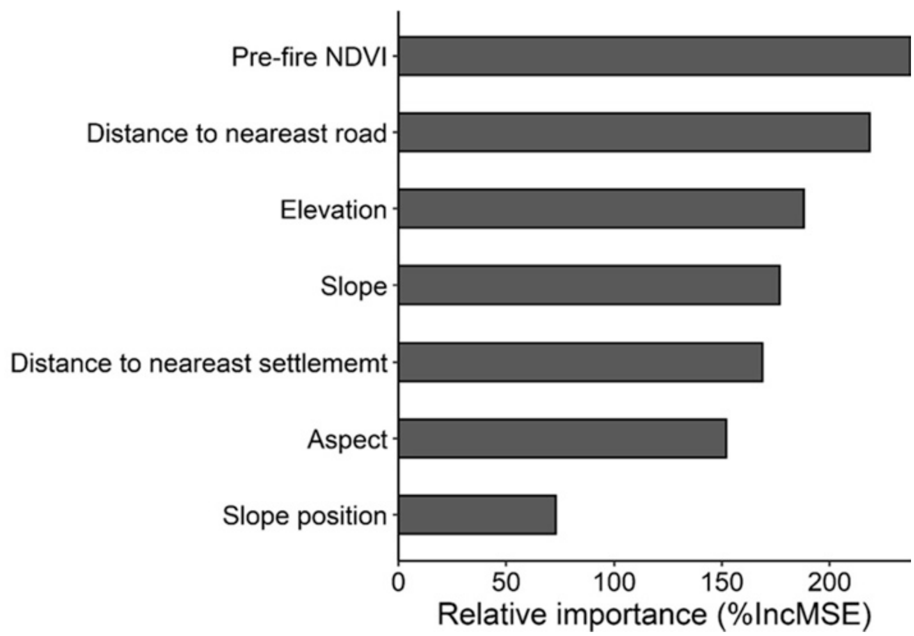

Fig. 6. Relative contributions of the predictor variables to the stability indicators in the random forest model denoted by the percentage increase in the mean squared error (%IncMSE).

affected the distribution pattern of burn severity. Moderate and high degrees of burned patches were mainly distributed in areas>1 km away from the nearest road, accounting for>70 % of the total burned area (Fig. 8). Because forest fires mostly occurred near the settlement in this area (Fig. A1), the area within 600 m from the nearest settlement was also the main distribution area of high burned patches (Fig. 7). Consistent with our prediction, burn severity had an obvious correlation with terrain distribution. The higher burn severity area was mainly concentrated on the sunny slope, higher altitude (>200 m), relatively gentle slope (<25°), and upper slope in our study area (Fig. 7). The statistical analysis results showed that in areas with a slope<25°, moderate and high burned patches accounted for 40 % and 22 % of the total area, respectively. The proportion of high burned severity on the upper slope was>30 %.

4. Discussion

4.1. Accuracy assessment of burn severity

This study compared the ability of a range of spectral indices in burn severity assessment and suggested that dNBR, RdNBR, and RBR are optimal spectral indices in fitting CBI values (Table 3), although dNBR was slightly higher in accuracy classification, especially for unburned and moderate severity assessment (Table 5). In previous studies, most results indicated the NBR-based indices are optimal in burn severity assessment (Cansler and McKenzie, 2012; Kurbanov et al., 2017; Parks et al., 2014; Saulino et al., 2020). In subtropical forest regions, a similar study by Veraverbeke et al. (2010) compared the ability of dNDVI, dNDMI, and dNBR to assess burn severity in forests of southern Greece, and dNBR was the best index among the three spectral indices. Cansler and McKenzie (2012) reported that RdNBR had a higher accuracy in burn severity assessment compared with the other indices in subalpine forests (overall accuracy = 62 %, kappa = 0.40). In the Mediterranean, dNBR and CBI were highly correlated (R^2 = 0.79), with an overall classification accuracy of 85 % (Kurbanov et al., 2017). In addition, NBR-based indices suggested higher burn severity assessment in tropical forests (Rozario et al., 2018) and boreal forests (Chang et al., 2015).

Our study indicated that the moderate degree was less accurately classified than the other degrees of burn severity based on spectral indices. This could be caused by misclassification between burned and newly grown green vegetation. Due to the warm and humid climate of subtropical forests, the rapid recovery of vegetation after a fire increases the difficulty of remote sensing-based classification and discrimination to a certain extent. Moreover, the decreased accuracy in the moderate class of burn severity might be explained by 'mixed pixels', in which the burn severity pattern presented high spatial variability (Hayes and

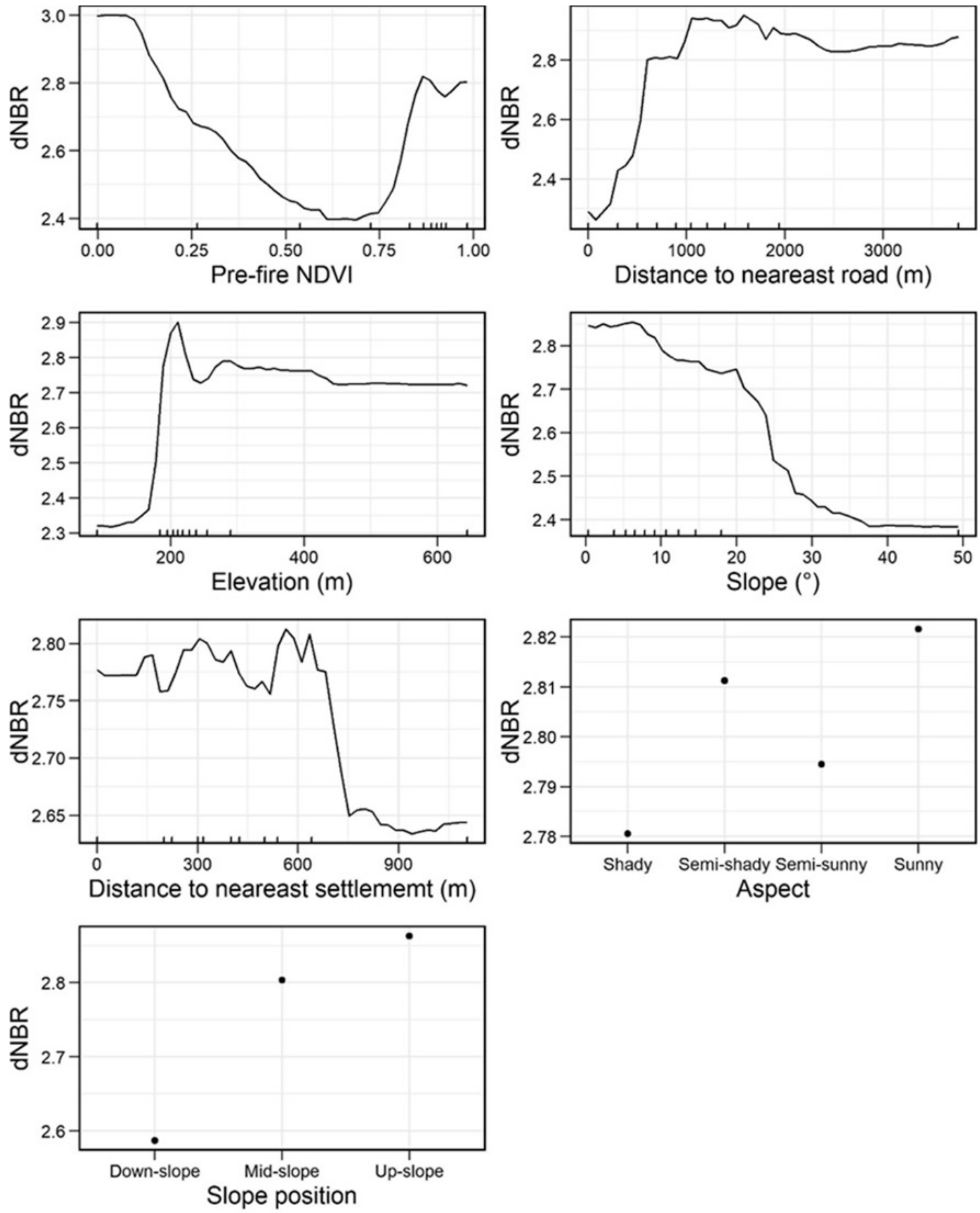

Fig. 7. Partial dependence plots for the random forest model run using the seven variables showing the response of burn severity to the individual predictor. The variables shown are pre-fire NDVI, elevation, distance to the nearest road, slope, distance to the nearest settlement, aspect, and slope position.

Robeson, 2011; Miller et al., 2009). Therefore, improvements in the identification and quantification of moderate burn severity depend on the development of spectral indices with higher spatial resolution (meter or sub-meter level imagery) (Fernández-Manso et al., 2016; van Gerrevink and Veraverbeke, 2021).

4.2. Spatial patterns and drivers of burn severity

Generally, moderate and low burn severity were predominant in subtropical forests of this area, and the spatial pattern of burn severity showed obvious heterogeneity because of the influence of topography, vegetation, and human activities. The distribution pattern of burn severity suggested that most low and moderate burn severity areas were concentrated at low altitudes, whereas high burn severity areas were mainly distributed at higher elevations, mostly above 500 m (Fig. 7 and Fig. 8). These distribution patterns were largely related to the predominance of anthropogenic fires in subtropical forests. Anthropogenic fires mostly occurred near settlements and roads at low altitudes; these fires are easy to detect and extinguish (Pourtaghi et al., 2016). They are thus less likely to spread over large areas or cause high burn severity.

As expected, spatial heterogeneity of burn severity was substantially explained by vegetation (Fig. 6). Our study suggested that most high

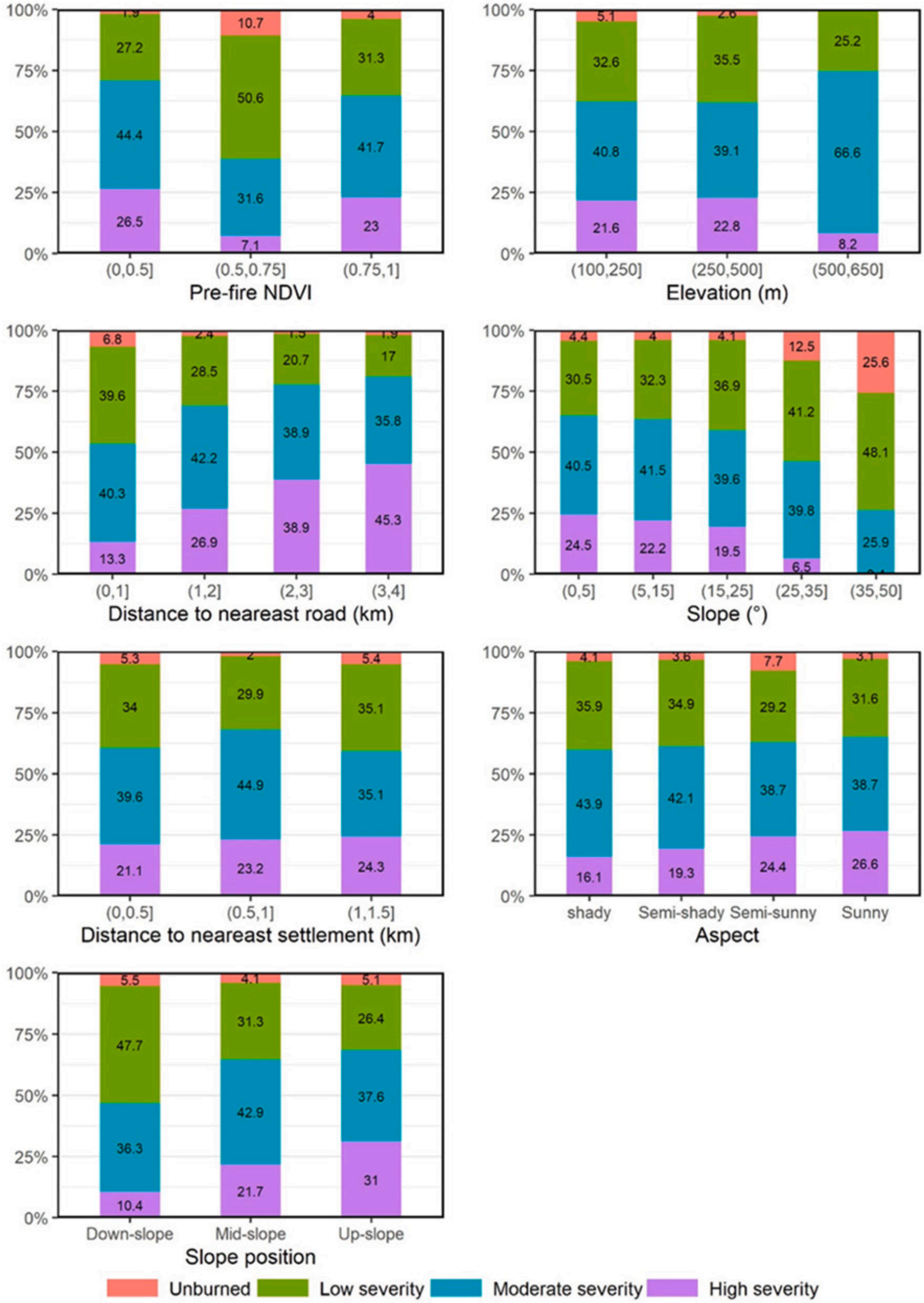

Fig. 8. Proportion of each burn severity class of the total burned area under various site factors.

burn severity occurred in areas of high pre-fire NDVI values. However, some areas with lower pre-fire NDVI values also had higher burn severity, which might be related to the heterogeneity of vegetation type or structures. For example, some open shrubs or coniferous forests have lower NDVI than closed broadleaved forests, but they tend to develop higher burn severity. Therefore, as important drivers of burn severity, more vegetation characteristics such as stand type and stand structure variables should be applied to the assessment of burn severity to further reveal the relationship between vegetation and burn severity (Birch et al., 2015). In this study, the influence of human activity (the distance to the nearest road) on burn severity was more important than the terrain factors (Fig. 6). Previous studies considered that human activities mainly affected the number of fire occurrences, but their impact on burn severity was rarely discussed (Liu et al., 2012; Su et al., 2019). In the subtropical forests of South China, human-caused fires were the main ones and mostly occurred near residential areas, and the accessibility of traffic largely affected burn severity. Our study demonstrated that in areas with a long distance from the nearest road, the proportion of high burn severity was obviously higher due to poor traffic accessibility (Fig. 7 and Fig. 8). Climate and meteorological conditions are important factors affecting burn severity, but they often affect and control on a large spatial scale (Wu et al., 2013). At the local scale, burn severity was more strongly influenced by topography and vegetation; thus, the influence of climate or meteorological drivers was not considered in this study (Birch et al., 2015).

5. Conclusions and management implications

We compared the ability of reflective, thermal, and mixed indices for evaluating burn severity in subtropical forests based on Landsat 8 OLI. This study demonstrated that dNBR, RdNBR, and RBR had high fitting accuracy in burn severity assessment of subtropical forests in Southern China. Among these optimal fitting indices, dNBR had a better classification accuracy (overall accuracy close to 60 %) in burn severity assessment. By using the dNBR index, we mapped burn severity in this study area, and further analyzed the spatial patterns and drivers of burn severity. Vegetation and human activities are the main drivers affecting the distribution of burn severity patterns. Areas with higher NDVI and farther distance from the nearest road were more likely to develop higher burn severity. Topography also had an important influence on the spatial distribution of burn severity, and high burn severity patches tend to be distributed in sunny, upper, and gentle slopes. Determining the optimal spectral indices for burn severity is of great significance to understand the spatial patterns and drivers of burn severity, thus providing a scientific basis for the management and prevention of forest fires in subtropical forest regions.

Most burned areas were close to residential areas and roads, which is a significant safety hazard for residents. Therefore, a fire isolation belt near settlements is necessary to minimize losses caused by forest fires (Cui et al., 2019). Under the climate change scenario, the risk of fire outbreaks and burn severity in subtropical regions will increase (Hijmans et al., 2005; Wu et al., 2019). Understanding the spatial patterns and drivers of burn severity in subtropical forests and combining them with previous fire spread models to better identify the environmental conditions more likely to develop low, moderate, or high burn severity can provide managers with effective fire risk management strategies. To make explicit recommendations for fire management, it is necessary to strengthen the monitoring and management of fuel through remote sensing technology, especially in areas with high NDVI values. Priority should be given to the removal of fuels and flammables from sunny slopes, uphill positions, and high elevation areas to reduce or avoid the occurrence of high burn severity. In addition, considering that high burn severity areas are prone to secondary fires because of the early vegetation restoration being mainly dominated by flammable shrubs (Bright et al., 2019), measures to prevent secondary fires should include thinning and the removal of combustible materials (García-Llamas et al., 2020).

CRediT authorship contribution statement

Lingling Guo: Methodology, Data curation, Writing – original draft. **Shun Li:** Conceptualization, Writing – review & editing, Supervision. **Zhiwei Wu:** Conceptualization, Methodology, Project administration, Funding acquisition. **Russell A. Parsons:** Supervision. **Shitao Lin:** . **Bo Wu:** . **Long Sun:** Writing – review & editing, Funding acquisition.

Declaration of Competing Interest

The authors declare that they have no known competing financial interests or personal relationships that could have appeared to influence the work reported in this paper.

Data availability

Data will be made available on request.

Acknowledgements

This study was funded by National Key R&D Program “Research on forest and grassland fire early warning and prevention technology and key equipment” (Project No. 2018YFE0207800).

Appendix A. Supplementary data

Supplementary data to this article can be found online at https://doi.org/10.1016/j.foreco.2022.120515.

References

Birch, D.S., Morgan, P., Kolden, C.A., Abatzoglou, J.T., Dillon, G.K., Hudak, A.T., Smith, A.M.S., 2015. Vegetation, topography and daily weather influenced burn severity in central Idaho and western Montana forests. Ecosphere (Washington D.C) 6, t17–t23. https://doi.org/10.1890/ES14-00213.1.

Bowd, E.J., Banks, S.C., Strong, C.L., Lindenmayer, D.B., 2019. Long-term impacts of wildfire and logging on forest soils. Nature Geosci 12, 113–118. https://doi.org/10.1038/s41561-018-0294-2.

Brewer, C.K., Winne, J.C., Redmond, R.L., Opitz, D.W., Mangrich, M.V., 2005. Classifying and Mapping Wildfire Severity. photogramm eng remote sensing 71, 1311–1320. https://doi.org/10.14358/PERS.71.11.1311.

Bright, B.C., Hudak, A.T., Kennedy, R.E., Braaten, J.D., Henareh Khalyani, A., 2019. Examining post-fire vegetation recovery with Landsat time series analysis in three western North American forest types. fire ecol 15, 11770. https://doi.org/10.1186/s42408-018-0021-9.

Broncano, M.J., Retana, J., 2004. Topography and forest composition affecting the variability in fire severity and post-fire regeneration occurring after a large fire in the Mediterranean basin. Int. J. Wildland Fire 13, 209. https://doi.org/10.1071/WF03036.

Cansler, C.A., McKenzie, D., 2012. How Robust Are Burn Severity Indices When Applied in a New Region? Evaluation of Alternate Field-Based and Remote-Sensing Methods. Remote Sensing 4, 456–483. https://doi.org/10.3390/rs4020456.

Cardil, A., Mola-Yudego, B., Blázquez-Casado, Á., González-Olabarria, J.R., 2019. Fire and burn severity assessment: Calibration of Relative Differenced Normalized Burn Ratio (RdNBR) with field data. Journal of environmental management 235, 342–349. https://doi.org/10.1016/j.jenvman.2019.01.077.

Chang, Y., Zhu, Z., Feng, Y., Li, Y., Bu, R., Hu, Y., 2016. The spatial variation in forest burn severity in Heilongjiang Province, China. Nat Hazards 81, 981–1001. https://doi.org/10.1007/s11069-015-2116-9.

Cui, X., Alam, M.A., Perry, G.L., Paterson, A.M., Wyse, S.V., Curran, T.J., 2019. Green firebreaks as a management tool for wildfires: Lessons from China. Journal of environmental management 233, 329–336. https://doi.org/10.1016/j.jenvman.2018.12.043.

De Keersmaecker, W., Lhermitte, S., Tits, L., Honnay, O., Somers, B., Coppin, P., 2015. A model quantifying global vegetation resistance and resilience to short-term climate anomalies and their relationship with vegetation cover. Glob. Ecol. Biogeogr. 24, 539–548. https://doi.org/10.1111/geb.12279.

Fang, L., Yang, J., Zu, J., Li, G., Zhang, J., 2015. Quantifying influences and relative importance of fire weather, topography, and vegetation on fire size and fire severity in a Chinese boreal forest landscape. Forest Ecology and Management 356, 2–12. https://doi.org/10.1016/j.foreco.2015.01.011.

Fernández-García, V., Beltrán-Marcos, D., Fernández-Guisuraga, J.M., Marcos, E., Calvo, L., 2022. Predicting potential wildfire severity across Southern Europe with global data sources. The Science of the total environment 829, 154729. https://doi.org/10.1016/j.scitotenv.2022.154729.

Fernández-Manso, A., Fernández-Manso, O., Quintano, C., 2016. SENTINEL-2A red-edge spectral indices suitability for discriminating burn severity. International Journal of Applied Earth Observation and Geoinformation 50, 170–175. https://doi.org/10.1016/j.jag.2016.03.005.

Fernández-Manso, A., Quintano, C., 2015. Evaluating Landsat ETM+ emissivity-enhanced spectral indices for burn severity discrimination in Mediterranean forest ecosystems. Remote Sensing Letters 6, 302–310. https://doi.org/10.1080/2150704X.2015.1029093.

Fu J., Wu Z., Yan S., Zhang Y., Gu X., Du., 2020. Effects of climate, vegetation, and topography on spatial patterns of burn severity in the Great Xing'an Mountains. Acta Ecologica Sinica. 40(5):1672-1682. DOI: 10. http://dx.doi.org/5846/stxb201902140264.

Gao, X., Huete, A.R., Ni, W., Miura, T., 2000. Optical-biophysical relationships of vegetation spectra without background contamination. Remote Sens. Environ. 74, 609–620. https://doi.org/10.1016/S0034-4257(00)00150-4.

García-Llamas, P., Suárez-Seoane, S., Fernández-Manso, A., Quintano, C., Calvo, L., 2020. Evaluation of fire severity in fire prone-ecosystems of Spain under two different environmental conditions. Journal of environmental management 271, 110706. https://doi.org/10.1016/j.jenvman.2020.110706.

Harvey, B.J., Donato, D.C., Turner, M.G., 2016. Drivers and trends in landscape patterns of stand-replacing fire in forests of the US Northern Rocky Mountains (1984–2010). Landscape Ecol 31, 2367–2383. https://doi.org/10.1007/s10980-016-0408-4.

Hayes, J.J., Robeson, S.M., 2011. Relationships between fire severity and post-fire landscape pattern following a large mixed-severity fire in the Valle Vidal, New Mexico, USA. Forest Ecology and Management 261, 1392–1400. https://doi.org/10.1016/j.foreco.2011.01.023.

Hijmans, R.J., Cameron, S.E., Parra, J.L., Jones, P.G., Jarvis, A., 2005. Very-high-resolution interpolated climate surfaces for global land areas. International Journal of Climatology 25, 1965–1978. https://doi.org/10.1002/JOC.1276.

Hijmans R., 2022. raster: Geographic Data Analysis and Modeling. R package version 3.5-15. https://CRAN.R-project.org/package=raster.

Jin, Q., Ma, X., Wang, W., Yang, X., Guo, F., 2017. Temporal and spatial characteristics of particulate matter emission from forest fires in Subtropical China during 2000—2014. Acta Scientiae Circumstantiae, 37(6) : 2238-2247. https://doi.org/10.13671 /j.hjkxxb.2017.0003.

Key, C.H., Benson, N.C., 2006. Landscape assessment: ground measure of severity, the composite burn index; and remote sensing of severity, the normalized burn ratio. FIREMON: Fire Effects Monitoring and Inventory System. USDA, Forest Service, Rocky Mountain Research Station General Technical Report RMRS-GTR-164-CD. LA1-LA51, Ogden, Utah.

Kurbanov, E., Vorobyev, O., Leznin, S., Polevshikova, Y., Demisheva, E., 2017. Assessment of burn severity in Middle Povozhje with Landsat multitemporal data. Int. J. Wildland Fire 26, 772. https://doi.org/10.1071/WF16141.

Lentile, L.B., Smith, F.W., Shepperd, W.D., 2006. Influence of topography and forest structure on patterns of mixed severity fire in ponderosa pine forests of the South Dakota Black Hills, USA. Int. J. Wildland Fire 15, 557. https://doi.org/10.1071/WF05096.

Liaw, A., Wiener, M., 2002. Classification and Regression by randomForest. R News 2 (3), 18–22. https://CRAN.R-project.org/doc/Rnews/.

Liu, Z., Yang, J., Chang, Y., Weisberg, P.J., He, H., 2012. Spatial patterns and drivers of fire occurrence and its future trend under climate change in a boreal forest of north-east China. Global Change Biology. 18, 2041–2056. https://doi.org/10.1111/J.13652486.2012.02649.X.

López-García, M.J., Caselles, V., 1991. Mapping burns and natural reforestation using thematic mapper data. Geocarto Int. 1, 31–37. https://doi.org/10.1080/10106049109354290.

Lorente, M., Parsons, W.F.J., McIntire, E.J.B., Munson, A.D., 2013. Wildfire and forest harvest disturbances in the boreal forest leave different long-lasting spatial signatures. Plant Soil. 364, 39–54. https://doi.org/10.1007/s11104-012-1331-3.

McLauchlan, K.K., Higuera, P.E., Miesel, J., Rogers, B.M., Schweitzer, J., Shuman, J.K., Tepley, A.J., Varner, J.M., Veblen, T.T., Adalsteinsson, S.A., Balch, J.K., Baker, P., Batllori, E., Bigio, E., Brando, P., Cattau, M., Chipman, M.L., Coen, J., Crandall, R., Daniels, L., Enright, N., Gross, W.S., Harvey, B.J., Hatten, J.A., Hermann, S., Hewitt, R.E., Kobziar, L.N., Landesmann, J.B., Loranty, M.M., Maezumi, S.Y., Mearns, L., Moritz, M., Myers, J.A., Pausas, J.G., Pellegrini, A.F.A., Platt, W.J., Roozeboom, J., Safford, H., Santos, F., Scheller, R.M., Sherriff, R.L., Smith, K.G., Smith, M.D., Watts, A.C., Durigan, G., 2020. Fire as a fundamental ecological process: Research advances and frontiers. J Ecol 108 (5), 2047–2069.

Miller, J.D., Thode, A.E., 2007. Quantifying burn severity in a heterogeneous landscape with a relative version of the delta Normalized Burn Ratio (dNBR). Remote Sensing of Environment 109, 66–80. https://doi.org/10.1016/j.rse.2006.12.006.

Miller, J.D., Knapp, E.E., Key, C.H., Skinner, C.N., Isbell, C.J., Creasy, R.M., Sherlock, J. W., 2009. Calibration and validation of the relative differenced Normalized Burn Ratio (RdNBR) to three measures of fire severity in the Sierra Nevada and Klamath Mountains, California, USA. REMOTE SENS ENVIRON 113, 645–656. https://doi.org/10.1016/j.rse.2008.11.009.

Parks, S., Dillon, G., Miller, C., 2014. A New Metric for Quantifying Burn Severity: The Relativized Burn Ratio. Remote Sensing 6, 1827–1844. https://doi.org/10.3390/rs6031827.

Pourtaghi, Z.S., Pourghasemi, H.R., Aretano, R., Semeraro, T., 2016. Investigation of general indicators influencing on forest fire and its susceptibility modeling using different data mining techniques. Ecological Indicators 64, 72–84. https://doi.org/10.1016/j.ecolind.2015.12.030.

R Core Team (2017) R: A language and environment for statistical computing. R Foundation for Statistical Computing. https://www.R-project.org.

Ramsey, M.S., Arrowsmith, J.R., 2001. New images of fire scars may help mitigate future natural hazards. Eos Trans. AGU 82 (36), 393.

Rouse, J.W., Haas, R.H., Schell, J.A., Deering, D.W., 1973. Monitoring vegetation systems in the great plains with ERTS. In: Proceedings of the Third ERTS Symposium. NASA SP-351, 1. NASA, Washington DC, U.S., pp. 309–317.

Rozario, P., Madurapperuma, B., Wang, Y., 2018. Remote Sensing Approach to Detect Burn Severity Risk Zones in Palo Verde National Park. Costa Rica. REMOTE SENS-BASEL 10, 1427. https://doi.org/10.3390/rs10091427.

Saulino, L., Rita, A., Migliozzi, A., Maffei, C., Allevato, E., Garonna, A.P., Saracino, A., 2020. Detecting Burn Severity across Mediterranean Forest Types by Coupling Medium-Spatial Resolution Satellite Imagery and Field Data. Remote Sensing 12 (4), 741.

Schwalm, C.R., Anderegg, W.R.L., Michalak, A.M., Fisher, J.B., Biondi, F., Koch, G., Litvak, M., Ogle, K., Shaw, J.D., Wolf, A., Huntzinger, D.N., Schaefer, K., Cook, R., Wei, Y., Fang, Y., Hayes, D., Huang, M., Jain, A., Tian, H., 2017. Global patterns of drought recovery. Nature 548, 202–205. https://doi.org/10.1038/nature23021.

Soverel, N.O., Perrakis, D.D.B., Coops, N.C., 2010. Estimating burn severity from Landsat dNBR and RdNBR indices across western Canada. Remote Sensing of Environment 114, 1896–1909. https://doi.org/10.1016/j.rse.2010.03.013.

Steel, Z.L., Koontz, M.J., Safford, H.D., 2018. The changing landscape of wildfire: burn pattern trends and implications for California's yellow pine and mixed conifer forests. Landscape Ecol 33, 1159–1176. https://doi.org/10.1007/s10980-018-0665-5.

Su, Z., Tigabu, M., Cao, Q., Wang, G., Hu, H., Guo, F., 2019. Comparative analysis of spatial variation in forest fire drivers between boreal and subtropical ecosystems in China. Forest Ecology and Management 454, 117669. https://doi.org/10.1016/j.foreco.2019.117669.

van Gerrevink, M.J., Veraverbeke, S., 2021. Evaluating the Near and Mid Infrared Bi-Spectral Space for Assessing Fire Severity and Comparison with the Differenced Normalized Burn Ratio. Remote Sensing 13, 695. https://doi.org/10.3390/rs13040695.

Veraverbeke, S., Verstraeten, W.W., Lhermitte, S., Goossens, R., 2010. Evaluating Landsat Thematic Mapper spectral indices for estimating burn severity of the 2007 Peloponnese wildfires in Greece. INT J WILDLAND FIRE 19, 558. https://doi.org/10.1071/WF09069.

Whitman, E., Parisien, M.-A., Thompson, D.K., Hall, R.J., Skakun, R.S., Flannigan, M.D., 2018. Variability and drivers of burn severity in the northwestern Canadian boreal forest. Ecosphere 9 (2), e02128.

Wu, Z., He, H.S., Liang, Y., Cai, L., Lewis, B.J., 2013. Determining relative contributions of vegetation and topography to burn severity from LANDSAT imagery. Environmental management 52, 821–836. https://doi.org/10.1007/s00267-013-0128-3.

Wu, Z., He, H.S., Keane, R.E., Zhu, Z., Wang, Y., Shan, Y., 2020. Current and future patterns of forest fire occurrence in China. Int. J. Wildland Fire 29, 104. https://doi.org/10.1071/WF19039.

Yu, G., Chen, Z., Piao, S., Peng, C., Ciais, P., Wang, Q., Li, X., Zhu, X., 2014a. High carbon dioxide uptake by subtropical forest ecosystems in the East Asian monsoon region. Proceedings of the National Academy of Sciences of the United States of America 111 (13), 4910–4915.

Yu, X., Guo, X., Wu, Z., 2014b. Land Surface Temperature Retrieval from Landsat 8 TIRS—Comparison between Radiative Transfer Equation-Based Method, Split Window Algorithm and Single Channel Method. Remote Sensing 6, 9829–9852. https://doi.org/10.3390/rs6109829.

Zheng, Z., Zeng, Y., Li, S., Huang, W., 2016. A new burn severity index based on land surface temperature and enhanced vegetation index. International Journal of Applied Earth Observation and Geoinformation 45, 84–94. https://doi.org/10.1016/j.jag.2015.11.002.

Zhu, Z., Key, C., Ohlen, D., Benson, N., 2006. Evaluate sensitivities of burn-severity mapping algorithms for different ecosystems and fire histories in the United States. In: Final Report to the Joint Fire Science Program. JFSP 01-1-4-12.